Highly integrated direct methanol fuel cell systems minimizing fuel loss with dynamic concentration control for portable applications

Youngseung Na[a,c], Federico Zenith[b], Ulrike Krewer[a,*]

[a] Institute of Energy and Process Systems Engineering, TU Braunschweig, Franz-Liszt-Str. 35, 38106 Braunschweig, Germany
[b] SINTEF Mathematics and Cybernetics, PO Box 4760 Sluppen, 7465 Trondheim, Norway
[c] International Max Planck Research School for Advanced Methods in Process and Systems Engineering, Sandtorstr. 1, 39106 Magdeburg, Germany

ARTICLE INFO

Keywords:
DMFC
Fuel cell systems
Process integration
Concentration control

ABSTRACT

Direct methanol fuel cell (DMFC) systems are mostly composed of massive water recycling devices such as coolers, condensers or mixers even for small and light portable applications. Integrated systems, where system components serve more than one function, can be equipped with fewer components and have a lighter weight than conventional ones. However, the process integration can also bring about significant methanol evaporation in separators, resulting in low fuel efficiency. The here presented highly integrated system can minimize methanol loss with optimized concentration control to improve efficiency. Two system variants are compared with regard to concentration, temperature, water recovery controllability and efficiency. The simulation results are compared with the previously published mingled-outlet system and validated with experiments.

1. Introduction

Portable electric devices, such as smartphones, laptops or wearable devices are required to operate for long time despite having small volume and light weight. Li-ion batteries are a possible solution for this restriction within a certain range. Especially when the desired operating time is longer than the battery can deliver, fuel cell systems can compete with batteries [12]. Beyond this operating time, fuel cells such as a direct methanol fuel cell (DMFC) are advantageous for small scale applications because of the high energy density of methanol as fuel [11]. For tiny systems, passive fuel-supply mechanisms are employed without actuating components such as pumps or condensers. Kim et al. [6] and Qian et al. [9] utilized pressurized carbon dioxide gas from electrochemical reactions to push the methanol solution into the anode channels without any pumps in DMFC systems [5,9]. Cao et al. [2] developed an air-breathing system to eliminate the air pump. Despite the size advantage, passive systems performed worse than active systems due to their unstable reactant supply, which slightly depends on environmental conditions [14].

DMFC systems show maximum performance when operated on a diluted methanol solution [1], which is generated by condensing water from the cathode effluent [3]; however, the optimal concentration in general depends on the drawn current. One way to reduce the size of active DMFC systems is integrating the system components: Na et al. [7] reduced the number of components with a time-sharing pumping method in which one pump supplies methanol solution or neat methanol in turn, not simultaneously. The sharing time depends on methanol concentration in the mixer, and a way to estimate or measure methanol concentration is necessary. Without a concentration sensor, Zenith et al. [16] got rid of two components by process integration of cathode and anode outlet (Fig. 1(b)) compared with a reference system (Fig. 1(a)) that had a single component for each function [15]. However, the integrated system has lower faradaic efficiency than the reference system due to a large amount of methanol evaporating at the mingled outlet.

In this study, the model of the mingled-outlet system in Fig. 1(b) is improved by accounting for liquid hold-up in the stack; this model is validated with experiments. Then the system is modified to the so-called highly integrated system and both are compared. The highly integrated system has an integrated unit combining a separator and a mixer, as shown in Fig. 2. To reduce potentially high methanol loss by evaporation in this unit (which is open to the environment), fuel is supplied after the separator and mixed in the tube with a static inline mixer. The portions of methanol crossover and evaporation are quantified by simulation as fuel loss.

* Corresponding author.
E-mail address: u.krewer@tu-braunschweig.de (U. Krewer).

Nomenclature

Latin symbols

a	crossover parameter [$\tilde{a} = 1.6748 \times 10^{-6}$ m/s]
A	active area [0.003 m^2]
b	crossover parameter [$\tilde{b} = 0.173$]
c	concentration [mol/m^3]
C_p	heat capacity [J/K]
E	energy [J]
F	Faraday constant [96,485 C/mol]
h	molar enthalpy [J/mol]
H	enthalpy [J]
I	current [A]
K	equilibrium constant [–]
K_c	proportional controller gain [–]
Δg_r	reaction Gibbs free energy [−702 kJ/mol]
Δh_r	reaction enthalpy [−726 kJ/mol]
M	molar mass [kg/mol]
N	number of cells [9]
n	amount of substance [mol]
p	pressure [Pa]
R	resistance [0.4 Ω]
s	Laplace variable [s^{-1}]
t	time [s]
T	temperature [K]
U	stack voltage [V]
U_0	open-circuit voltage [V]
V	volume [m^3]
W	weight [g]
x	liquid mole fraction [–]
y	gas mole fraction [–]
z	overall mole fraction [–]

Greek symbols

β	vaporisation ratio [–]
η	overall efficiency [–]
ν	stoichiometric coefficient, anodic reaction [–]
ξ	stoichiometric coefficient, crossover [–]
φ	faradaic efficiency [–]
λ	excess ratio [–]
π	vapour pressure [Pa]
ρ	density [kg/m^3]
σ	conditional integration flag [–]
τ	time constant [s]
τ_I	integral time [s]

Superscripts

air	air
an	anode
cath	cathode
eva	evaporation
env	environment
fuel	fuel
mix	mixer
sep	separator
sol	solution
stack	stack

Subscripts

d	electro-osmotic water drag
gas	gas
in	inlet
liq	liquid
out	outlet
PI	proportional-integral control
r	reaction
x	crossover

Diacritics

$\dot{\circ}$	flow [s^{-1}]
$\tilde{\circ}$	estimate [–]
$\bar{\circ}$	set point [–]

2. Modelling

The model of the mingled-outlet system from the research of Zenith et al. [16] assumed that liquid solution accumulates only in the mixer. This assumption is modified by adding a liquid hold-up in the anode channel of the stack. A larger stack is employed in this study to investigate actual response of fuel cell systems in the power range of several dozen watts. To implement the modified assumption into the model, liquid and gas are assumed to equilibrate in the anode channels of the stack according to the pressure equilibrium.

The highly integrated system inherits several components from the mingled-outlet system such as a fuel cell, a cooler and so on, except the integrated separator. The separator in the highly integrated system features material hold-up as a buffer, which was the function of the mixer in the mingled-outlet system.

The control strategy of the new system is combined with the dynamic concentration control scheme of the two-mixer system presented in Na et al. [8] and the stack temperature controller from the mingled-outlet system.

2.1. Cell stack

In DMFCs, methanol is oxidized on the anode (1) and water is produced on the cathode (2) as follows:

$$CH_3OH + H_2O \rightarrow CO_2 \uparrow + 6H^+ + 6e^- \tag{1}$$

$$6H^+ + 6e^- + \frac{3}{2}O_2 \rightarrow 3H_2O \tag{2}$$

The stack model, including reactions, mass transport and equilibrium equations, is based on the reference system model [15]. Methanol consumption in stacks is attributed to electrochemical reaction and methanol crossover through the membrane.

First, methanol reacts proportionally to electric current I and the number of the cells N in the stack:

$$\dot{n}_r = \frac{NI}{6\mathrm{F}} \tag{3}$$

where F is Faraday's constant.

Second, the flow rate of methanol crossover through the membrane is related to bulk concentration c^{an} in anode channels and electric current I:

$$\dot{n}_x = N\left(aAc^{\mathrm{an}} - \frac{b}{6\mathrm{F}}I\right) \tag{4}$$

where crossover parameters a and b depend on stack temperature [4], and A is the active area of the stack.

The voltage is assumed linear with current and modelled with Thévenin's equivalent circuit, which is calibrated in the experiment at the operating temperature of 60 °C.

$$U = U_0 - RI \tag{5}$$

To implement material hold-up in the anode channel of the stack, the reaction and accumulation process are virtually separated. First, the species mass balances, including anodic reaction

(1), are calculated as in the reference system [15]. Next, the gas–liquid equilibrium in the anode is calculated: assuming that only methanol and water can be present in liquid phase, the molar vaporisation rate can be calculated analytically with the Rachford-Rice equation [13], which becomes a second-order polynomial; the liquid and vapour compositions x_j and y_j are then calculated from overall compositions z_j and the molar vaporisation ratio. Liquid and gas volume are calculated with liquid density and ideal gas law, respectively.

The gaseous CO_2 generated by the anodic reaction (1) has a very low density, and displaces liquid from the anode channels through the stack outlet; this can have significant effects when current is rapidly changed. The total volume of liquid and gas phases is constrained to the inner volume V^{stack} of the anode channels in the stack.

$$V_{\text{gas}}^{\text{stack}} + V_{\text{liq}}^{\text{stack}} = V^{\text{stack}} \tag{6}$$

Material and energy balance of each species in the anode channel as virtual reservoir are calculated separately from the stack reaction.

2.2. Integrated separator

The integrated separator splits gas and liquid flows from the sum of cathode and anode outlets, similar to the separator in the mingled-outlet system of Fig. 1(b); in addition, it is modified with a liquid and energy hold-up.

Incondensable components leave the separator from the gas outlet only, whereas methanol and water leave from both liquid and gas outlets; the gas–liquid equilibrium is solved through the Rachford-rice equation, just like in Section 2.1.

The material and energy hold-ups of the integrated separator are implemented similarly to the mixer of the reference and mingled-outlet systems.

2.3. Balance of plant

The cooler model is identical to that of the mingled-outlet system [16]: it merges methanol, water and carbon dioxide from anode outlet with water, oxygen and nitrogen from cathode outlet. Pumps and blowers are modelled to supply the exact amount of fluids as requested by controllers with no time lags. The inline mixer is designed only for the experiment to blend neat methanol uniformly with the methanol solution, like in the simulations.

2.4. Efficiency definitions

Faradaic efficiency φ is the fraction of methanol that reacts in the anodic reaction (1), i.e. the ratio of consumed methanol in the anode (proportional to current I) to the total methanol provided to the system:

$$\varphi = N \frac{I}{6\mathrm{F}} \frac{1}{\dot{n}^{\text{fuel}}} \tag{7}$$

The overall efficiency η is the ratio of the power provided by the stack to the reaction enthalpy Δh_r contained in the supplied methanol $\dot{n}^{\text{fuel}}$:

$$\eta = \frac{I\,U}{\dot{n}^{\text{fuel}}\,\Delta h_r} \tag{8}$$

2.5. Concentration estimator

It has been found previously that the dynamics of anodic methanol concentration is stable, and that therefore it is possible to use an estimator for anodic methanol concentration instead of a direct measurement [15]. This estimation is used to implement feedforward control on the same anodic methanol concentration.

The estimated moles of methanol in the system is calculated with the sum of four terms: the incoming neat methanol from the fuel tank $\dot{n}^{\text{fuel}}$, the rate of methanol consumption in the anode $\dot{n}_r$, the rate of methanol crossover $\dot{n}_x$, and the methanol loss in the separator $\dot{n}_{\text{CH}_3\text{OH}}^{\text{eva}}$:

$$\frac{\mathrm{d}\tilde{n}_{\text{CH}_3\text{OH}}^{\text{mix(}or\ \ \text{sep)}}}{\mathrm{d}t} = \dot{n}^{\text{fuel}} - \dot{n}_r - \dot{n}_x - \dot{n}_{\text{CH}_3\text{OH}}^{\text{eva}} \tag{9}$$

The amount of methanol lost in the separator is calculated as follows:

$$\dot{n}_{\text{CH}_3\text{OH}}^{\text{eva}} = \overbrace{\dot{n}_{\text{air}}\left(1 - \frac{y_{\text{O}_2}^{\text{env}}}{3\lambda^{\text{cath}}}\right)}^{\text{Air flow}} \frac{K_{\text{CH}_3\text{OH}}}{1 - K_{\text{H}_2\text{O}}} \overbrace{\frac{\tilde{c}^{\text{mix(}or\ \ \text{sep)}} \cdot M_{\text{H}_2\text{O}}}{\rho_{\text{H}_2\text{O}}}}^{\text{CH}_3\text{OH mole fraction}} \tag{10}$$

where the air flow rate is meant at the mingled outlet and the methanol mole fraction is meant in diluted methanol solution. $\dot{n}_{\text{CH}_3\text{OH}}^{\text{eva}}$ is approximately calculated with equilibrium constants of methanol $K_{\text{CH}_3\text{OH}}$ and water $K_{\text{H}_2\text{O}}$ [16].

Given the estimated moles of methanol in the anodic loop $\tilde{n}_{\text{CH}_3\text{OH}}^{\text{mix}}$, the concentration $c^{\text{mix(}or\,\text{sep)}}$ is obtained dividing it by the solution volume $\bar{V}^{\text{mix}}$, which is assumed to be measurable.

$$\tilde{c}^{\text{mix(}or\ \text{sep)}} = \frac{\tilde{n}_{\text{CH}_3\text{OH}}^{\text{mix(}or\ \text{sep)}}}{\bar{V}^{\text{mix(}or\ \text{sep)}}} \tag{11}$$

2.6. Controller synthesis

To increase faradaic efficiency in comparison with the mingled-outlet system, the highly integrated system employs the optimizing concentration controller introduced in the two-mixer system [8] in order to minimise methanol loss in the separator. Air flow rate and solution volume controllers are inherited from the reference system, like in the case of the mingled-outlet system [16].

2.6.1. Concentration controller

Methanol concentration in the anodic loop and stack temperature are controlled by manipulating the solution and fuel flow rates with a multi-input, multi-output (MIMO) controller. This MIMO controller is based on the concept of combining the dynamic concentration controller from the two-mixer system [8] and the stack-temperature controller by manipulating the solution flow from the mingled-outlet system [16].

The target methanol concentration is set to maintain a constant faradaic efficiency φ by Eq. (7), similarly to the two-mixer system. In contrast to the latter system, methanol evaporation cannot be neglected in the highly integrated system, because the anodic outlet solution directly contacts a much larger amount of gas from the cathode outlet in the separator. Therefore, methanol evaporation in Eq. (10) is also considered to estimate methanol loss in the highly integrated system.

Concentration $\tilde{c}^{\text{sep}}$ in the integrated separator is calculated with estimated methanol amount $\tilde{n}_{\text{CH}_3\text{OH}}^{\text{sep}}$ and measured solution volume $\bar{V}^{\text{sep}}$ in the separator by Eq. (11).

The target anode inlet concentration is determined by the target faradaic efficiency φ and anodic reactant excess ratio λ^{an}:

$$\tilde{c}_{\text{in}}^{\text{an}} = \frac{I}{6F}\left(\frac{1}{\varphi} + \tilde{b} - 1\right)\frac{1}{\tilde{a}A}\frac{\lambda^{\text{an}}}{\lambda^{\text{an}} - 1} \tag{12}$$

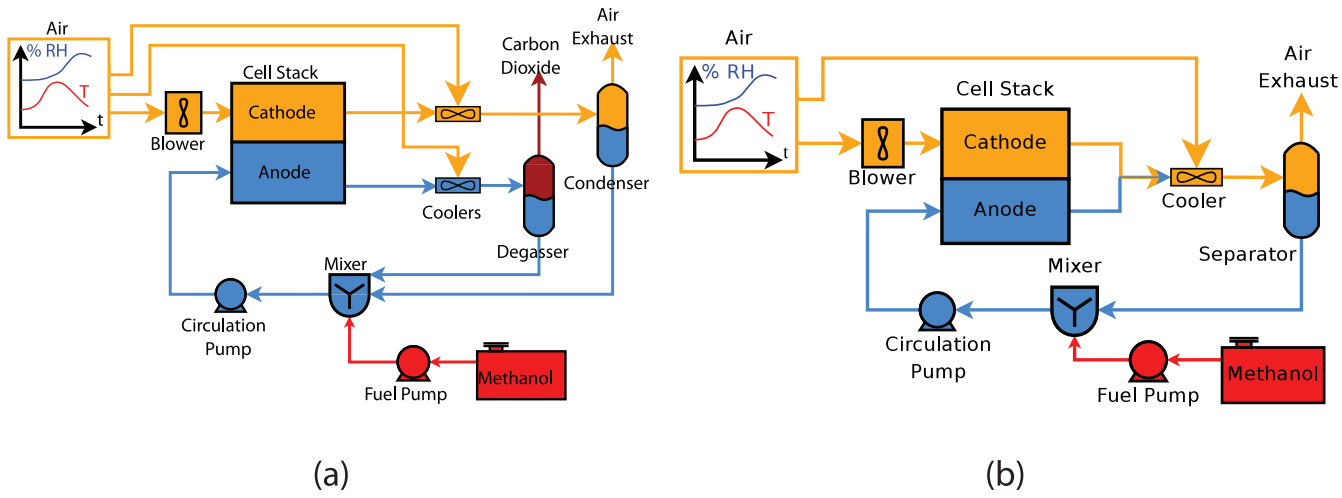

Fig. 1. The process scheme of (a) the reference system [15] and (b) the mingled-outlet system [16].
Reprinted from *Chemical Engineering and Processing*, **59**, p44 (2012), Copyright 2012, with permission from Elsevier.

The solution flow to the anode is set so that the net methanol feed is λ^{an} times the consumption by reactions and evaporation:

$$\dot{V}_{\lambda}^{an} = \frac{\lambda^{an}}{\bar{c}_{in}^{an}} \left\{ N \left[\frac{I}{6F}(1-\tilde{b}) + \tilde{a} A \tilde{c}^{sep} \right] + \dot{n}_{CH_3OH}^{eva} \right\} \tag{13}$$

When the set concentration $\bar{c}_{in}^{an}$ is lower than the estimated concentration $\tilde{c}^{sep}$, the fuel flow rate is set to zero to quickly reduce the concentration in the anodic loop; otherwise, both methanol and solution flow rates are determined by species mass balance:

$$\begin{cases} \bar{c}_{in}^{an} \left(\dot{V}^{fuel} + \dot{V}^{sol} \right) = \dfrac{\rho_{CH_3OH}}{M_{CH_3OH}} \dot{V}^{fuel} + \tilde{c}^{sep} \dot{V}^{sol} & \text{if} \quad \tilde{c}^{sep} < \bar{c}_{in}^{an} \\ \dot{V}^{fuel} = 0 & \text{otherwise} \end{cases} \tag{14}$$

2.6.2. Temperature controller

Another manipulated variable, solution volume flow $\dot{V}_{PI}^{an}$, controls stack temperature with proportional-integral (PI) control, like in the mingled-outlet system.

$$\dot{V}_{PI}^{an} = K_c(\bar{T}^{stack} - T^{stack}) + \int \sigma \frac{K_c}{\tau_I}(\bar{T}^{stack} - T^{stack}) dt \tag{15}$$

The proportional gain K_c and integral time constant τ_I are obtained from Eqs. (16) and (17), where τ_c is the desired response time [10]:

$$K_c = -\frac{C_p^{stack}}{\tau_c C_{p,H_2O} \Delta T} \tag{16}$$

$$\tau_I = 4\tau_c \tag{17}$$

The two values $\dot{V}_{\lambda}^{an}$ and $\dot{V}_{PI}^{an}$ will in general be different; the former is set to avoid reactant starvation, and the latter regulates stack temperature. Since reactant starvation is a much faster and more critical condition than temperature deviations, the former is given priority and set as an absolute minimum for the actual value of $\dot{V}^{sol}$. The resulting equation is therefore:

$$\dot{V}^{an} = \dot{V}^{fuel} + \dot{V}^{sol} = \max\left(\dot{V}_{\lambda}^{an}, \dot{V}_{PI}^{an} \right) \tag{18}$$

In Eq. (15), the conditional integration flag σ is equal to 1 when $\dot{V}_{PI}^{an}$ is dominating and 0 otherwise, to avoid wind-up in the PI controller.

2.6.3. Solution volume controller

To provide enough water to dilute neat methanol down to the set concentration, a sufficient amount of diluted solution should be maintained in the integrated separator. Liquid is recovered from water condensation in the cooler, whose temperature is set with a gain-scheduled P controller previously developed for the reference system [15].

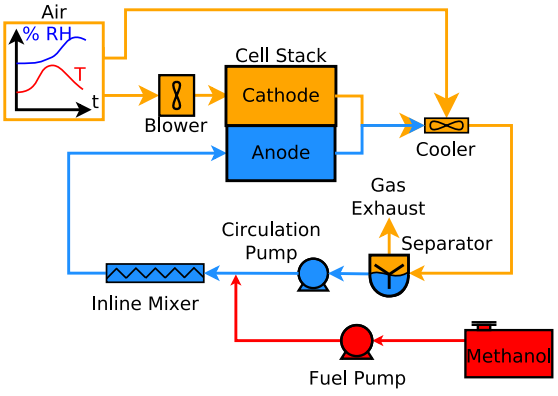

Fig. 2. The process scheme of the highly integrated system.

3. Experiment

Simulation of the system is validated by experiments with the same control algorithm. The mingled-outlet system [16] is validated, and the experiments of the highly integrated system are executed with identical operating conditions as of the model.

3.1. Experimental setup

The condenser and the cathodic cooler of the reference system [15] are removed in the mingled-outlet system [16], as shown in Fig. 1(b). Furthermore, the system is placed in a climate chamber (PL-3KPH, ESPEC, Japan). The anodic cooler and the degasser function as loop cooler and separator. In the highly integrated system, the integrated separator is designed in-house (Fig. 3): it separates liquid from gas and weighs the solution hold-up with a strain gauge (FSH01483, Futek, Germany). A porous medium with more than 80% of porosity covers the top of the separator to avoid liquid splash. An in-line static mixer (Plastic Mixer 103201, ESSKA.de GmbH, Germany) blends methanol solution and neat methanol in a tube before the anode inlet, similarly to the two-mixer system [8]. R/S-type thermocouples measure temperature at 6 points in the tubes, located at the inlets and outlets of cooler, anode

Table 1
Synthesized controllers for the highly integrated system.

Manipulated variable	Controller
Air flow rate	$\dot{V}_{\text{in}}^{\text{air}} = \lambda^{\text{cath}} N \frac{RT^{\text{env}}}{p^{\text{env}} y_{\text{O}_2}^{\text{env}}} \left(\frac{3}{2} aA\bar{c}^{\text{sep}} + \frac{1-b}{4\text{F}} I \right)$ [16]
Separator temperature	$\delta\bar{T}^{\text{sep}} = \left[\tau_c \frac{\hat{n}^{\text{air}}}{p^{\text{env}}} \frac{d\pi_{\text{H}_2\text{O}}(T^{\text{sep}})}{dT^{\text{sep}}} \right]^{-1} \frac{\rho_{\text{H}_2\text{O}}}{M_{\text{H}_2\text{O}}} \delta V^{\text{sep}}$ [15]
Fuel flow rate	$\dot{V}^{\text{fuel}} = \begin{cases} \frac{\bar{c}_{\text{in}}^{\text{an}} - \bar{c}^{\text{sep}}}{\rho_{\text{CH}_3\text{OH}}/M_{\text{CH}_3\text{OH}} - \bar{c}^{\text{sep}}} \max(\dot{V}_{\lambda}^{\text{an}}, \dot{V}_{PI}^{\text{an}}) & \text{if } \bar{c}^{\text{sep}} < \bar{c}_{\text{in}}^{\text{an}} \\ 0 & \text{otherwise} \end{cases}$
Solution flow rate	$\dot{V}^{\text{sol}} = \begin{cases} \frac{\rho_{\text{CH}_3\text{OH}}/M_{\text{CH}_3\text{OH}} - \bar{c}_{\text{in}}^{\text{an}}}{\rho_{\text{CH}_3\text{OH}}/M_{\text{CH}_3\text{OH}} - \bar{c}^{\text{sep}}} \max(\dot{V}_{\lambda}^{\text{an}}, \dot{V}_{PI}^{\text{an}}) & \text{if } \bar{c}^{\text{sep}} < \bar{c}_{\text{in}}^{\text{an}} \\ \max(\dot{V}_{\lambda}^{\text{an}}, \dot{V}_{PI}^{\text{an}}) & \text{otherwise} \end{cases}$

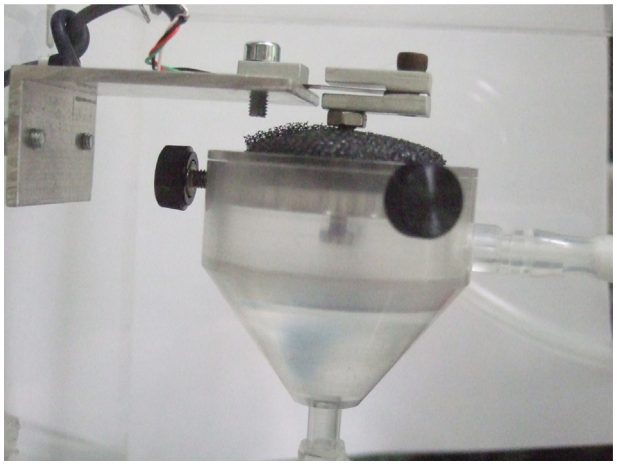

Fig. 3. Combined tank mixer and separator.

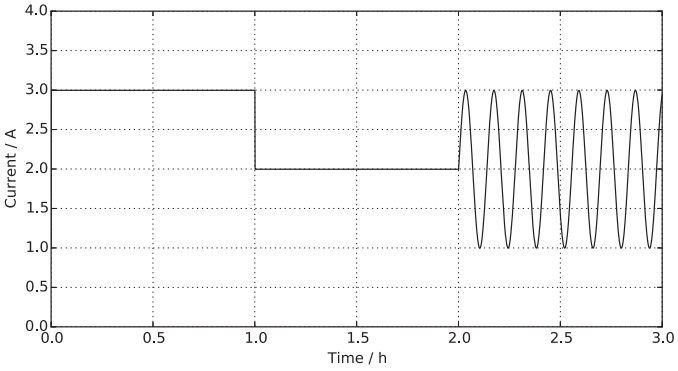

Fig. 4. Input current to the DMFC stack in all different systems.

and cathode; a K-type thermocouple measures the stack temperature. Concentrations are measured by a density meter (MCS, ISSYS, U.S.A.) after the separator. An electric load (ZS512-4SV20NV, H&H, Germany) draws current and measures the voltage of the DMFC stack. Pneumatic and hydraulic devices are equipped with pumps and mass flow controllers. A peristaltic pump (Reglo Digital, Ismatec, Switzerland) supplies neat methanol to the in-line mixer and another peristaltic pump with an Easy-Load pumping head (MCP Standard, Ismatec, Switzerland) circulates methanol solution in the anodic loop. Compressed air flows through mass flow controllers (SmartTrak C100, U.S.A.) for cathode reaction and cooling of the heat exchanger (custom-built, IMM, Germany) to condense water vapour. The DMFC stack (15W balticFuelCells, Germany) is composed of 9 cells with 30 cm^2 of active area per each cell. During the whole test, data points are sampled every second with a LabVIEW device (cRIO compact, National Instrument, U.S.A). The controllers synthesised in Section 2.6 are implemented in LabVIEW as the explicit forms listed in Table 1.

3.2. Operating conditions

The preconditioning of system temperature and concentration in the anodic loop to steady state is similar to that of the reference system. The initial temperature of the system is set to 50 °C; the climate chamber fixes the temperature at 37 °C and retains it for over an hour until each system component reaches uniform temperature. During preheating, concentration is set to 1 M in the separator, and current to 1 A to activate the stack. After this initial setting, electric current is drawn according to the reference profile shown in Fig. 4 for 3 h: first, 3 A current is drawn for 1 h, while flow rates are controlled by the aforementioned controllers in the modelling section; next, the current drops down to 2 A to identify the dynamic response of the system, and maintained for 1 h. Finally, the current oscillates from 1 A to 3 A with a pre-set sinusoidal curve with a period of 500 s for 1 h. Each controller of the mingled-outlet system or the highly integrated system operates autonomously according to the current disturbance.

3.3. Error analysis

The error ranges of thermocouples are ±1.0 K (R/S type) and ±1.5 K (K type). For the weight of the solution in the separator, the strain gauge has error range ±0.25% at room temperature. It is calibrated at the environmental temperature of 25 °C so that the maximum error at 45 °C is ±1.0%. The resolution of the voltage measurement lies within ±0.02%, with monitoring voltage offset ±15 mV. Concentration error in the density meter is ±0.30% by weight, which is automatically calibrated in the device against temperature variation.

4. Results and discussions

4.1. Mingled outlet system validation

The mingled-outlet system is operated experimentally to validate and compare both the previous model and the newly proposed one with material hold-up in the stack. The dynamic behaviours of stack temperature, methanol concentration in the anodic loop and solution weight in the mixer are compared for the different models. The voltage profiles of the stack in the experiment and the simulation are similar to each other, as shown in Fig. 5.

As shown in Fig. 6, first, stack temperature starts at 50 °C and rises up to 60 °C in 15 min. After 15 min, all the temperatures remain

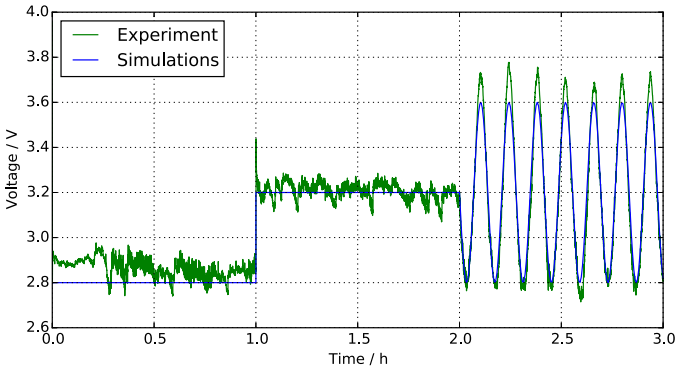

Fig. 5. Voltage response of the DMFC stack to the current input of Fig. 4 in the mingled-outlet system.

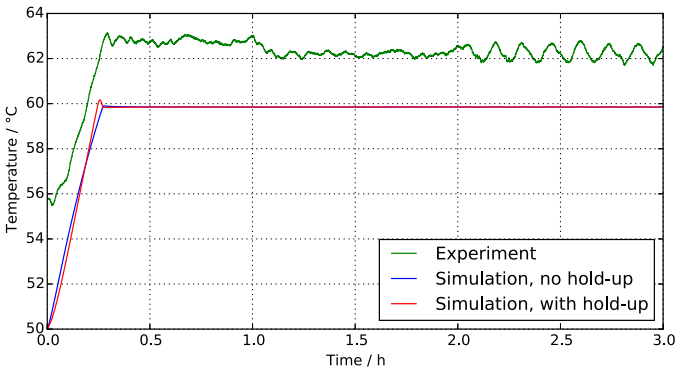

Fig. 6. Stack temperature profiles of the mingled-outlet system.

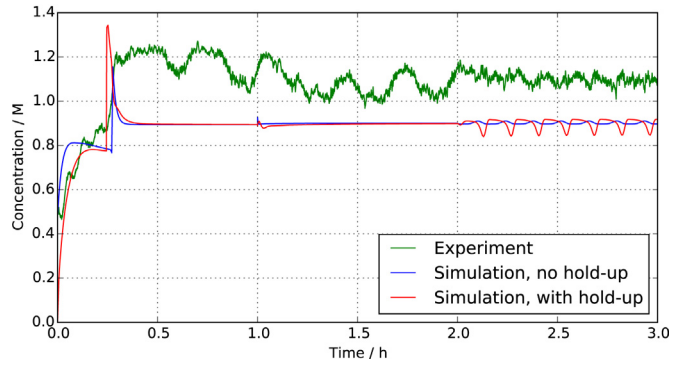

Fig. 7. Concentration profiles at the outlet of the separator in the mingled outlet system.

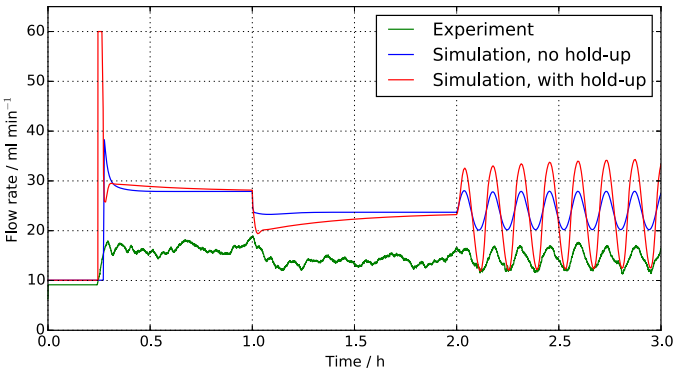

Fig. 8. Solution flow rate into the anode inlet of the mingled-outlet stack.

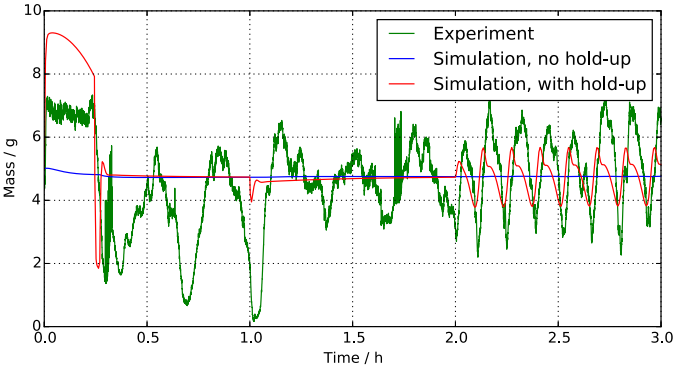

Fig. 9. Solution weight profiles at the mixer in the mingled-outlet system.

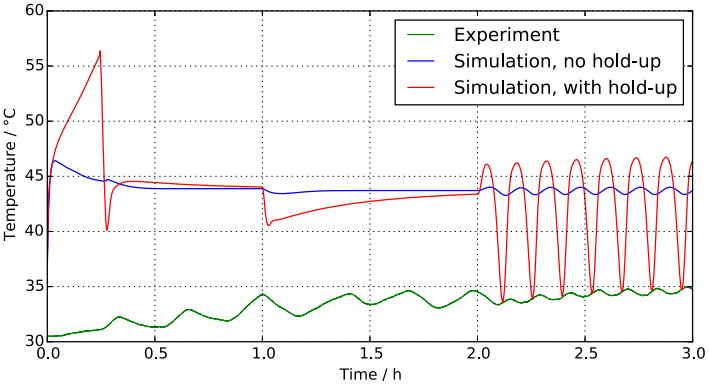

Fig. 10. Mixer temperature profiles of the mingled-outlet system.

steady until the end of the operation. The temperature control algorithm works successfully in all simulations. The small temperature offset between experiment and simulation is attributed to higher experimental methanol concentration in the anodic loop, as seen in Fig. 7.

After stack temperature exceeds the set temperature, $\dot{V}_{PI}^{an}$ overtakes $\dot{V}_{\lambda}^{an}$ at 15 min (Fig. 8). The change of active control law for flow results in the peak concentration shown in Fig. 7. The dynamic behaviour of stack temperature of the proposed model is similar to the previous model's. However, the mixer solution volume behaves very differently because of the liquid hold-up in the anode channel, as shown in Fig. 9. The larger solution volume at the beginning dampens the dynamics of mixer methanol concentration, which mitigates the slope of concentration increase (Fig. 7). The concentration peak of the proposed model is higher than the other's because the solution volume in the mixer at that time is lowest. After the peak, the outlet concentration of the proposed model stabilizes slightly below 1 M.

In the experiment, concentration settles at a higher value than in simulations because of the lower temperature in the mixer (see Fig. 10), due to the fact that the real system is not perfectly insulated; this reduces methanol loss compared to the simulation.

For the same reason, the solution flow rate into the anodic inlet in the experiment is smaller than in the simulations. The solution flow rate of PI controller $\dot{V}_{PI}^{an}$ is calculated by Eqs. (15) and (16), and K_c is proportional to the inverse of the temperature difference between the stack and the mixer. In the experiment, stack temperature is higher and mixer temperature is lower than in the simulations. The larger temperature difference results in smaller K_c and $\dot{V}_{PI}^{an}$, as shown in Fig. 8.

The significant difference between the models with and without hold-up is solution accumulation. As shown in Fig. 9, when a high current of 3A is drawn at the beginning, the water contained in the

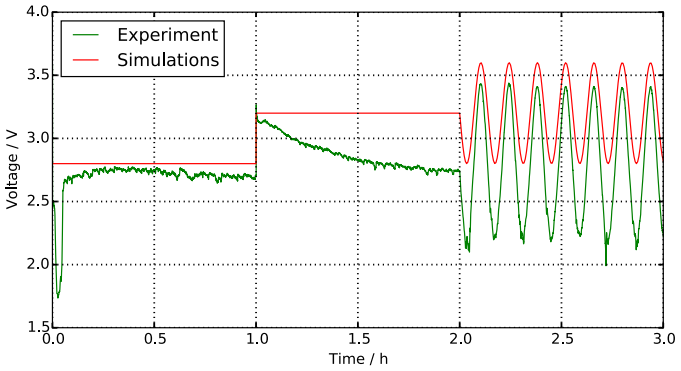

Fig. 11. Voltage response of the stack to the current input in the highly integrated system.

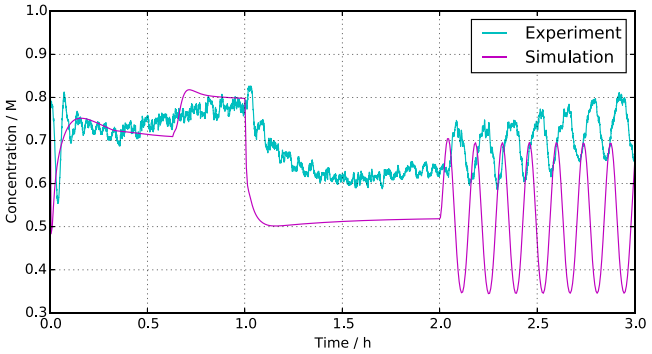

Fig. 13. Concentration profiles at the outlet of the separator in the highly integrated system.

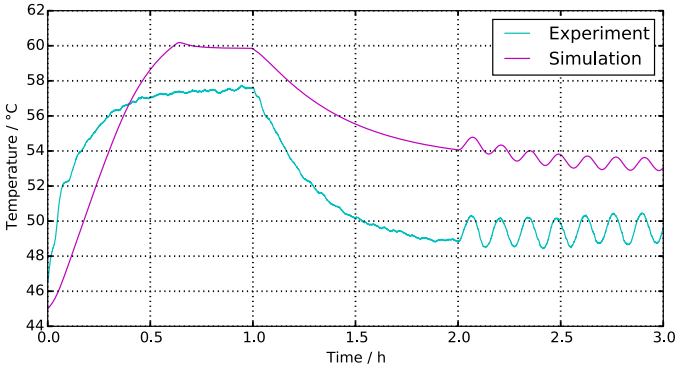

Fig. 12. Stack temperature profiles of the highly integrated system.

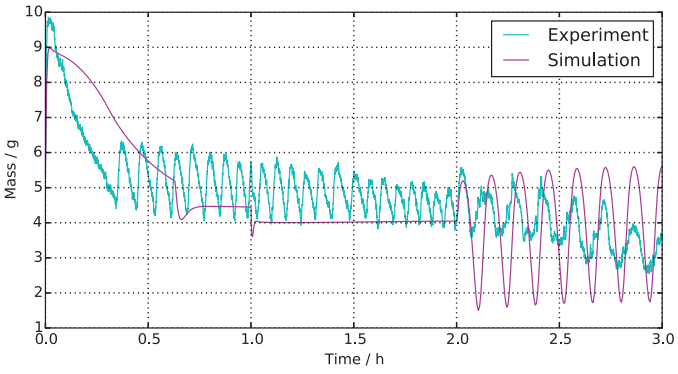

Fig. 14. Solution weight profiles at the tank buffer in the highly integrated system.

anodic channels of the stack flowed out to the mixer and inflated its solution volume for 15 min. After 15 min, when the solution flow rate suddenly increases as control is passed from $\dot{V}_{\lambda}^{\mathrm{an}}$ to $\dot{V}_{PI}^{\mathrm{an}}$, liquid solution in the mixer almost depletes because of the material hold-up in the anode channel.

Solution volume V^{mix} fluctuates vigorously in the experiment because it is directly influenced by solution flow rate $\dot{V}^{\mathrm{an}}$; when the latter is used to control stack temperature, $\dot{V}_{PI}^{\mathrm{an}}$ fluctuates as an effect of feedback control.

Comparing the two simulation results, the amount of solution in the mixer hardly changes when subject to sinusoidal current in the previous model; the experiment and the new model shows high-amplitude sinusoidal responses. The oscillations in volume are caused by the increased production of CO_2 in the anode at higher currents, which rapidly displaces liquid to the mixer: the new model is able to capture this experimentally observed effect.

4.2. Highly integrated system

As in previous models, the voltage profile of this model is calculated by a Thévenin's equivalent circuit, independent from the operating temperature of the stack and methanol concentration, and this is not meant to produce an accurate prediction of voltage. Fig. 11 shows that experimental results feature lower voltage than the simulation, which is explained by the lower stack temperature that is obtained in the experiment: at low currents, insufficient heat is generated to maintain the desired stack temperature, as visible in Fig. 12. In a commercial, compact system, this is not likely to be an issue, since the tightly insulated and integrated component will maintain heat better than our laboratory setup.

In the experiment, concentration is measured after separation because the sensor cannot operate on a two-phase flow: the measurement is therefore lower than the actual anode outlet concentration because of methanol evaporation in the separator. In the starting region, concentration reaches a minimum after a few seconds (Fig. 13), which is caused by the fast load change from 1A to 3A. The sudden current increase causes methanol starvation at the catalyst layer until the highly concentrated solution compensates for it. After an hour, the concentration profile from the experimental result is higher than that of the simulation because of overestimated methanol crossover. While the control parameters for the estimation of methanol crossover $\tilde{a}$ and $\tilde{b}$ are calibrated at 60 °C, the actual crossover is reduced by the lower temperature of the stack (see Fig. 12).

The solution buffer in the experiment is not located only in the stack and mixer as in the simulations: the liquid in tubes and the cooler mitigates rapid concentration changes. Therefore, the concentration profile in the experiment is not as steep as in the simulation, but shows a smooth curve after the current step after 1 h.

The initial peak of solution weight (see Fig. 14) results from liquid hold up: when the current steps up from 1A to 3A just after start-up, the produced carbon dioxide gas immediately pushes out liquid from the stack, raising the solution weight from 5g to 10g in a short time. After reaching the set value after about 1 h, the solution weight profile in the simulation converges to the steady state, whereas the one from the experimental results oscillates within an amplitude of about 2g because of the two phase volume change in the cooler. Shrinking gas volume after cooling slowed down solution flow rate to the integrated separator. This volume change of gas in the cooler did not affect solution volume in the other systems because buffers such as a separator, a degasser or a condenser mitigate sudden changes. If the cooler is modelled with material hold-up for two phase mixture, it may be able to simulate volume contraction of gas precisely in the future. In a real system, a heat

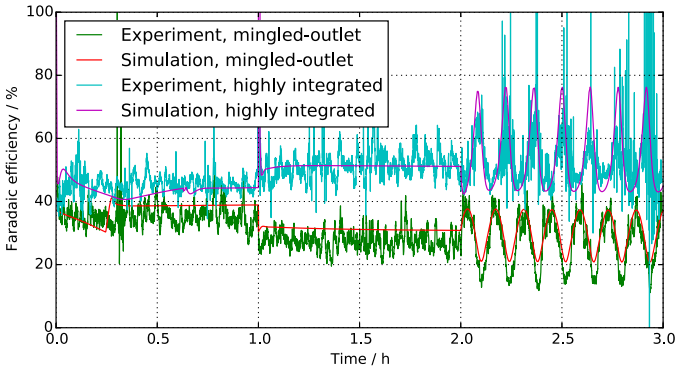

Fig. 15. Fuel efficiencies of the mingled-outlet system and the highly integrated system.

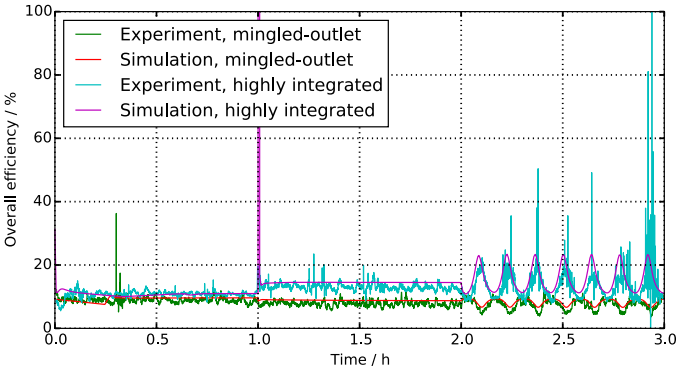

Fig. 16. Overall efficiencies of the mingled-outlet system and the highly integrated system.

exchanger with high heat exchanging efficiency or small heat mass can reduce the solution weight fluctuation.

4.3. Efficiency

In the experiment, the fuel tank was weighed by an electric scale to calculate methanol consumption. The discontinuous pumping of the peristaltic pump disturbs the sensitive balance, producing noise as visible in Fig. 15. Over the whole period, the highly integrated system has higher faradaic efficiency than the mingled-outlet system due to optimized concentration control (Fig. 13), which leads to less methanol loss. This holds not only for experiments but also for simulations, which matched the experiments very well. In the simulation, methanol evaporation is separately calculated from methanol crossover loss. 20.5% and 29.5% of supplied methanol evaporates in the highly integrated and the mingled-outlet systems respectively over the whole period.

The overall efficiency profile is slightly different from faradaic efficiency as shown in Fig. 16. During the whole period, the highly integrated system is more efficient than the mingled-outlet system because of the optimal concentration control, especially at lower current. The small gap between model and experiment in the highly integrated system at the current 2A (from 1–2 h) results from the lower voltage at the lower temperature.

5. Conclusions

In previous research, the mingled-outlet system was suggested as a simplification of the reference system, which however had lower efficiency due to high methanol evaporation in the separator: this also constrains the use of portable DMFC systems to the outdoors.

The simulation of the mingled-outlet system model has been validated, and experiments are executed with the same parameters and controllers as in the simulations. In the experiments, the solution volume is not only accumulated in the mixer, but also in the stack's anode channels, in tubing and other units. The stack model, modified with material hold-up in the anode channels, was able to estimate the dynamic behaviour of the solution weight closer to the experimental result than the previous model.

The highly integrated system is proposed for higher efficiency and fewer components than the mingled-outlet system, integrating the mixer and the separator. The compact design of the highly integrated system is appropriate for portable applications such as laptops or leisure power sources, though in general the overall efficiency is relatively small.

Despite its compactness and higher efficiency compared to the mingled-outlet system, the highly integrated system still has disadvantages due to non-negligible methanol evaporation compared to conventional systems (such as the reference system) and low tolerance to rapid current increases, which can cause temporary methanol starvation. When dynamic load tracking is necessary, the target Faradaic efficiency can be marginally lowered or the load ramp-up rate can be moderated to prevent starvation, possibly by hybridisation with buffer batteries.

Acknowledgements

This research was supported by grant KR3850/1-1 from DFG program (Germany) for the project "Analysis and Design of Portable and Autonomous Direct Methanol Fuel Cell Systems".

References

[1] Srikanth Arisetty, Cedric A. Jacob, Ajay K. Prasad, Suresh G. Advani, Regulating methanol feed concentration in direct methanol fuel cells using feedback from voltage measurements, J. Power Sources 187 (2) (2009) 415–421.
[2] Jianyu Cao, Zhiqing Zou, Qinghong Huang, Ting Yuan, Zhilin Li, Baojia Xia, Hui Yang, Planar air-breathing micro-direct methanol fuel cell stacks based on micro-electronic-mechanical-system technology, J. Power Sources 185 (1) (2008) 433–438.
[3] Christopher K. Dyer, Fuel cells for portable applications, J. Power Sources 106 (1) (2002) 31–34.
[4] T. Kallio, K. Kisko, K. Kontturi, R. Serimaa, F. Sundholm, G. Sundholm, Relationship between methanol permeability and structure of different radiation-grafted membranes, Fuel Cells 4 (4) (2004) 328–336.
[5] HaeKyoung Kim, Passive direct methanol fuel cells fed with methanol vapor, J. Power Sources 162 (2) (2006) 1232–1235.
[6] Joon-Hee Kim, Min-Jee Yang, Jun-Young Park, Improvement on performance and efficiency of direct methanol fuel cells using hydrocarbon-based membrane electrode assembly, Appl. Energy 115 (2014) 95–102.
[7] Youngseung Na, Jungmin Kwon, Hyun Kim, Hyejung Cho, Inseob Song, Characteristics of a direct methanol fuel cell system with the time shared fuel supplying approach, Energy 50 (2013) 406–411.
[8] Youngseung Na, Federico Zenith, Ulrike Krewer, Increasing fuel efficiency of direct methanol fuel cell systems with feedforward control of the operating concentration, Energies 8 (9) (2015) 10409–10429.
[9] Weimin Qian, David P. Wilkinson, Jun Shen, Haijiang Wang, Jiujun Zhang, Architecture for portable direct liquid fuel cells, J. Power Sources 154 (1) (2006) 202–213.
[10] Sigurd Skogestad, Simple analytic rules for model reduction and PID controller tuning, J. Process Control 13 (4) (2003) 291–309.
[11] Kai Sundmacher, Keith Scott, Direct methanol polymer electrolyte fuel cell: analysis of charge and mass transfer in the vapour–liquid–solid system, Chem. Eng. Sci. 54 (13) (1999) 2927–2936.
[12] Tony M. Thampan, Dinesh O. Shah, Clifford Cook, Jonathan Novoa, Sunil N. Shah, Development and evaluation of portable and wearable fuel cells for soldier use, J. Power Sources 259 (2014) 276–281.
[13] Curtis H. Whitson, Michael L. Michelsen, The negative flash, Fluid Phase Equilib. 53 (1989) 51–71.
[14] Yuming Yang, Yung C. Liang, A direct methanol fuel cell system with passive fuel delivery based on liquid surface tension, J. Power Sources 165 (1) (2007) 185–195.
[15] Federico Zenith, Ulrike Krewer, Modelling, dynamics and control of a portable DMFC system, J. Process Control 20 (5) (2010) 630–642.
[16] Federico Zenith, Youngseung Na, Ulrike Krewer, Effects of process integration in an active direct methanol fuel-cell system, Chem. Eng. Process.: Process Intensif. 59 (2012) 43–51.